

Structural and Spectroscopic Analysis of the F393H Mutant of Flavocytochrome P450 BM3[†]

Tobias W. B. Ost,^{*,‡} Andrew W. Munro,[§] Christopher G. Mowat,^{*,||} Paul R. Taylor,^{||} Antonio Pessegueiro,[⊥] Armand J. Fulco,[⊥] Arthur K. Cho,[#] Myles A. Cheesman,[▽] Malcolm D. Walkinshaw,^{||} and Stephen K. Chapman[‡]

Department of Chemistry, University of Edinburgh, West Mains Road, Edinburgh, EH9 3JJ, U.K., Department of Biochemistry, The Adrian Building, University of Leicester, University Road, Leicester LE1 7RH, U.K., ICMB, University of Edinburgh, Mayfield Road, Edinburgh, EH9 3JR, U.K., Department of Biological Chemistry, UCLA School of Medicine, P.O. Box 951737, Los Angeles, California 90095-1737, Department of Molecular and Medical Pharmacology, UCLA School of Medicine, P.O. Box 951735, Los Angeles, California 90095-1735, School of Chemical Sciences, University of East Anglia, Norwich, NR4 7TJ, U.K.

Received April 9, 2001; Revised Manuscript Received September 4, 2001

ABSTRACT: In the preceding paper in this issue [Ost, T. W. B., Miles, C. S., Munro, A. W., Murdoch, J., Reid, G. A., and Chapman, S. K. (2001) *Biochemistry* 40, 13421–13429], we have established that the primary role of the phylogenetically conserved phenylalanine in flavocytochrome P450 BM3 (F393) is to control the thermodynamic properties of the heme iron, so as to optimize electron-transfer both to the iron (from the flavin redox partner) and onto molecular oxygen. In this paper, we report a detailed study of the F393H mutant enzyme, designed to probe the structural, spectroscopic, and metabolic profile of the enzyme in an attempt to identify the factors responsible for causing the changes. The heme domain structure of the F393H mutant has been solved to 2.0 Å resolution and demonstrates that the histidine replaces the phenylalanine in almost exactly the same conformation. A solvent water molecule is hydrogen bonded to the histidine, but there appears to be little other gross alteration in the environment of the heme. The F393H mutant displays an identical ferric EPR spectrum to wild-type, implying that the degree of splitting of the iron *d* orbitals is unaffected by the substitution, however, the overall energy of the *d*-orbitals have changed relative to each other. Magnetic CD studies show that the near-IR transition, diagnostic of heme ligation state, is red-shifted by 40 nm in F393H relative to wild-type P450 BM3, probably reflecting alteration in the strength of the iron-cysteinate bond. Studies of the catalytic turnover of fatty acid (myristate) confirms NADPH oxidation is tightly coupled to fatty acid oxidation in F393H, with a product profile very similar to wild-type. The results indicate that gross conformational changes do not account for the perturbations in the electronic features of the P450 BM3 heme system and that the structural environment on the proximal side of the P450 heme must be conformationally conserved in order to optimize catalytic function.

The cytochromes P450¹ are a family of monooxygenase enzymes implicated in a wide variety of biosynthetic and degradative pathways in organisms throughout nature (1–3). One essential feature shared by all P450s is a cysteine-ligated *b*-type heme (protoporphyrin IX) cofactor (4). Replacement of this cysteine residue results in a lack of heme

incorporation yielding catalytically inactive enzyme (5). Sequence comparisons of P450s clearly illustrate the implicit conservation of this cysteine throughout the P450 superfamily. It has been proposed that the electron-donating character of this residue facilitates the stabilization of the putative Fe^{IV}=O oxyferryl reactive species (6, 7) and, hence, is considered as an integral structural and mechanistic feature required by P450s.

Although overall topology is common to all of the structurally characterized P450s, the degree of sequence identity is often quite low between members (<25% amino acid identity) (8). However, investigations into a number of highly conserved residues over a range of P450s (primarily those of P450 cam—the camphor hydroxylase from *Pseudomonas putida*, and P450 BM3—the fatty acid hydroxylase from *Bacillus megaterium*) indicate their necessity for controlling aspects of the P450 catalytic cycle. For example, residues homologous to Thr252 of P450cam are implicated in providing a hydrogen bond to ferrous-bound molecular oxygen, participating in oxy-ferrous complex stabilisation (9). Also, a tryptophan residue (Trp96 in P450 BM3)

[†] This work is a contribution from the Edinburgh Protein Interaction Centre (EPIC) funded by the Wellcome Trust and the BBSRC (T.W.B.O.). The authors would like to thank Prof. A. J. Thomson for the use of the MCD and EPR facilities at the School of Chemical Sciences, U.E.A., with support from the BBSRC and EPSRC through core funding to the Centre for Metalloprotein Spectroscopy and Biology (CMSB) under Grant BO1727.

* To whom correspondence should be addressed. Phone: +44 131 6507386. Fax: +44 131 6504760. E-mail: skc03@holyrood.ed.ac.uk.

[‡] Department of Chemistry.

[§] Department of Biochemistry.

^{||} ICMB.

[⊥] Department of Biological Chemistry.

[#] Department of Molecular and Medical Pharmacology.

[▽] School of Chemical Sciences.

¹ Abbreviations: P450, cytochrome P450 monooxygenase; MCD, magnetic circular dichroism; GC/MS, gas chromatography/mass spectrometry; NOS, nitric oxide synthase.

interacting with the heme-propionates encourages heme binding and has been shown to have a controlling influence over the spin-state of the heme (10). The fact that the number of implicitly conserved residues common to all P450s constitutes only a small proportion of a "typical" P450 polypeptide infers that they are essential for catalytic competence and, hence, an evolutionary prerequisite.

Our previous study (11) has shown that substitution of one of these highly conserved residues, phenylalanine 393 (by alanine or histidine), in P450 BM3 results in a mutant form with appreciably different catalytic characteristics to wild-type. We have postulated this residue to be vital in controlling the reaction of the heme iron with molecular oxygen. The few examples in which this phenylalanine is not conserved fall into a small group of P450s which do not have to activate molecular oxygen. Examples of these are allene oxide synthase (Cyp74) (12), divinyl ether synthase (Cyp74) (13), prostacyclin synthase (Cyp8) (14), and thromboxane synthase (\sim Cyp3) (15). In all cases, the phenylalanine is substituted by either proline or tryptophan. Unlike typical P450s, these enzymes do not function as monooxygenases and do not require molecular oxygen or NAD(P)H-dependent P450 reductase for activity. These enzymes catalyze rearrangement or isomerization reactions, for which the activation of molecular oxygen is non-essential. This provides additional, yet unsubstantiated, evidence that this phenylalanine residue is intimately involved in steps in the P450 catalytic cycle, concerned with the binding and activation of molecular oxygen. The focus of our previous study (11) identified and characterized the catalytic differences of a series of F393-mutant enzymes, relative to wild-type. In this paper, we have attempted to resolve the origin of these perturbations to the kinetic and thermodynamic profile of wild-type P450 BM3 by focusing on spectroscopic and structural inspection of the mutant enzyme P450 BM3 F393H.

EXPERIMENTAL PROCEDURES

Escherichia coli Strains and Protein Preparation. Plasmids encoding the intact wild-type (pBM23), F393H (pCM37), and the heme domain of wild-type (pBM20) and F393H (pCM81) mutant enzymes were used to transform *Escherichia coli* strain TG1 (11). Cell growth and the extraction and purification of protein followed the same protocol as described previously (16).

Product Characterization. The products of the catalytic turnover of myristic acid (tetradecanoic acid) by wild-type P450 BM3 and F393H mutant were determined using gas chromatography/mass spectrometry according to the following methodology. A Hewlett-Packard 5971A GC/MS utilizing electron impact ionization (70 eV) instrument was used to determine structural information on the monohydroxylated metabolites of myristic acid. Metabolites were generated by incubation of 120 μ M myristate in the presence of 5 mM NADPH and a catalytic amount of P450 (ca. 1 nM) in 2 mL samples of 100 mM K_2HPO_4/KH_2PO_4 , pH 8. The metabolites were extracted into diethyl ether and converted to their methyl ester derivatives using diazomethane, before analysis by GC/MS. Chromatography of the samples was performed on a HP-35 capillary column (30 m \times 0.25 mm id \times 0.25 μ M film thickness) with a thermal gradient beginning at 100

Table 1: Characteristic Retention Times and Fragmentation Patterns of Myristate Metabolites Used to Identify the Site of Substrate Hydroxylation^a

position of hydroxylation retention time (min)	$\omega-1$ 24.66	$\omega-2$ 24.54	$\omega-3$ 24.23
fragment	<i>m/z</i>	<i>m/z</i>	<i>m/z</i>
M – CH ₃ (CH ₂) _{n-1}	243	229	215
M – CH ₃ (CH ₂) _{n-1} CH ₂ OH	211	197	183
M – CH ₃ (CH ₂) _{n-1} CHO	214	200	186

^a The conditions under which these data were generated is described in the Experimental Procedures.

°C for 0.5 min and increasing to 200 °C at a rate of 5 °C/min for 5 min and then to a final temperature of 250 °C at a rate of 10 °C/min. Injector temperature was set to 250 °C and the GC/MS transfer line was set at 280 °C. Column flow rate was set at 0.76 mL/min.

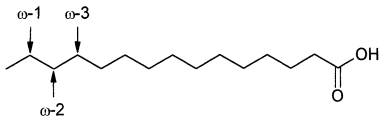
The mass spectra of the products from the control run (wild-type P450 BM3) were used to identify each GC peak. Monohydroxylated products were identified by their characteristic fragmentation pattern as shown in Table 1. The distribution of products was based on the relative peak area of the gas chromatogram, in which the total ion current was used to assess quantity.

UV–Vis Spectroscopy of Exogenous Ligand-Binding. The binding characteristics of azide, cyanide, imidazole, and pyridine (all from Aldrich and to the highest purity possible) to P450 BM3 wild-type and the F393H mutant were investigated. Protein concentrations in all cases were $<5 \mu$ M and were made up to 1 mL of total volume (100 mM MOPS, pH 7.0) in a 1 mL quartz cuvette (10 mm path length). Final ligand concentrations were no greater than 1.0 mM. The visible spectra of the ligand-bound P450s were taken in both the ferric- and ferrous-forms. Reduction was achieved by the addition of a few grains of dithionite to the cuvette. All spectrophotometric measurements were conducted using a Shimadzu 2101 Spectrophotometer at 25 °C.

MCD and EPR Spectroscopy. EPR spectra were recorded on an EPR spectrometer comprising an ER-200D electromagnet and microwave bridge interfaced to an EMX control system (Bruker Spectrospin) and fitted with a liquid helium flow cryostat (ESR-9, Oxford Instruments) and a dual-mode X-band cavity (Bruker, type ER4116DM). MCD spectra were recorded using circular dichrographs, JASCO models J-500D and J-730 for the UV–vis and near-infrared regions, respectively. An Oxford Instruments superconducting solenoid with a 25 mm ambient temperature bore was used to generate a magnetic field of 6 T for the room temperature MCD measurements. Room temperature MCD intensities are linearly dependent on magnetic field and are plotted normalized to magnetic field as $\Delta\epsilon/H$ ($M^{-1} cm^{-1} T^{-1}$).

Crystallography and Determination of the Crystal Structure of the F393H Heme Domain. Crystallization of F393H-HD (heme domain) was carried out by hanging drop vapor diffusion at 4 °C in Linbro plates. Crystals were obtained with a well solution comprising 100 mM sodium PIPES (piperazine-*N,N'*-bis[2-ethanesulfonic acid]), pH 6.5, 40 mM $MgSO_4$, 18–21% PEG 8000. Hanging drops of 4 μ L were prepared by adding 2 μ L of 41.7 mg/mL protein (in 50 mM TrisHCl/1 mM EDTA, pH 7.4) to 2 μ L of well solution. Plates of up to 1 \times 0.3 \times 0.3 mm were formed after about 1 week.

Table 2: Relative Proportions of Different Hydroxylated Metabolites from the Reactions of Wild-Type and F393H Mutant Flavocytochromes P450 BM3 with Myristic Acid^a

				
ENZYME	ω -1	ω -2	ω -3	Unreacted
P450 BM3 WT	53.6	24.5	20.0	1.9
P450 BM3 F393H	57.7	22.5	15.0	4.8

^a Products were determined as described in the Experimental Procedures.

Crystals were immersed in well solution containing 22% glycerol as a cryoprotectant, before being mounted in nylon loops and flash-cooled in liquid nitrogen. A data set was collected to 2.0 Å ($\lambda = 1.3$ Å) on station 9.5 at Daresbury synchrotron source using a MAR CCD detector. The crystals are isomorphous with those of the hemoprotein domain of wild-type flavocytochrome P450 BM3, with space group $P2_1$ and cell dimensions $a = 58.8$ Å, $b = 153.0$ Å, $c = 61.4$ Å, and $\beta = 94.7^\circ$ and have two molecules in the asymmetric unit. This compares with unit cell dimensions of $a = 59.4$ Å, $b = 154.0$ Å, $c = 62.2$ Å, and $\beta = 94.7^\circ$ obtained for crystals of wild-type heme domain (17).

Data processing was carried out using the HKL package (18). The wild-type flavocytochrome P450 BM3 heme domain structure (2HPD), stripped of water, was used as the initial model. Electron density fitting was carried out using the program O (19). Restraints for the heme group were calculated from the CNS parameter file. Structure refinement was carried out using SHELX-97 (20). The atomic coordinates have been deposited in the Protein Data Bank (1JME).

RESULTS

Product Characterization. It is well established that wild-type P450 BM3 displays strict substrate-specificity for long-chain fatty acids, performing hydroxylation in a highly regio-specific manner. For wild-type enzyme, the sole hydroxylation products of palmitic acid are the ω -1, ω -2, and ω -3 hydroxy derivatives (21, 22). The same trend has been demonstrated here for the hydroxylation of myristate (Table 2) by the F393H mutant.

Previously reported substrate-binding characteristics of the F393H mutant enzyme indicated that its affinity for long-chain fatty acids was insensitive to the nature of the residue at position 393 (11). This mutant shows comparable affinity toward laurate and arachidonate as wild-type ($K_d = \sim 250$ and ~ 4 μ M, respectively). Characterization of the F393H-mediated turnover of myristate reveals an identical product profile to wild-type, indicating that both the substrate specificity and the regiospecificity of hydroxylation is unaffected by the F393H substitution. There is a virtually identical product profile to wild-type, although there appears to be a slightly higher proportion of the ω -1 metabolite with respect to the ω -3 product for F393H compared to wild-type. Notwithstanding this, the trend in regiospecificity between wild-type and the F393H mutant is the same (ω -1: ω -2: ω -3:unreacted = 28:13:11:1 (12:5:3:1), respectively). There is a slightly higher proportion of unreacted

myristate in the case of F393H turnover, resulting from the lower overall catalytic activity in this mutant, i.e., the F393H mutant turns over less myristate in the same time period as wild-type.

The important result is that the substitution of phenylalanine 393 by histidine results in a mutant-form that retains the same selectivity for long-chain fatty acids and displays the same regiospecificity of hydroxylation as wild-type P450 BM3.

Ligand Binding. Figure 1 shows the spectral characteristics of azide, cyanide, imidazole, and pyridine binding to wild-type (Figure 1a) and the F393H mutant (Figure 1b). The key features of the ferric, ferric ligand-bound and ferrous ligand-bound spectra are shown in Table 3.

For the F393H mutant, the ferrous spectrum in the presence of azide is identical to the ferrous, ligand-free spectra, the generation of which (in aerobic conditions) is only feasible due to its increased reduction potential. A similar argument can be made when pyridine is ligated. The F393H mutant displays a 19 nm red-shift ($423 \rightarrow 442$ nm) in the Soret absorption upon reduction of the ferric-pyridine complex. The wild-type ferric-pyridine complex can also be generated, but addition of dithionite fails to form the ferrous-pyridine form. This reflects the very negative wild-type heme reduction potential (-427 mV) compared to the more positive value (-332 mV) for the F393H mutant. This is substantiated by the ferrous-cyanide complex, where a shift in the Soret absorption peak ($440 \rightarrow 437$ nm) is observed (100% conversion) for F393H, yet incomplete conversion is observed ($\sim 50\%$) for wild-type. The ferrous-cyanide complex of wild-type seems to be intermediate between the ferric and ferric-cyanide complex, probably as a consequence of incomplete heme reduction.

Magnetic Circular Dichroism (MCD) Spectroscopy. The room-temperature UV-vis electronic spectrum of the F393H mutant is shown in Figure 2a, with its visible MCD spectrum in Figure 2b. Features at wavelengths 300–600 nm are due to π - π^* transitions of the porphyrin ring. Mixing of porphyrin- π with iron- d levels occurs to the extent that the spectra become diagnostic of the spin- and oxidation-state of the metal ion. This is especially so in the MCD where the spectroscopic changes are most pronounced (23, 24). At these wavelengths, the room-temperature MCD of F393H is almost identical in form to that of the WT P450 BM3 heme-domain (25).

The most informative low-spin ferric heme MCD feature is a positive-signed porphyrin (π)-to-ferric (d) charge transfer transition, the exact energy of which varies systematically with changes in axial ligation (26). In the room temperature near-infrared MCD of F393H (Figure 2c), this charge-transfer band is at ~ 1085 nm, a red-shift of ~ 40 nm relative to the WT heme-domain.

Electron Paramagnetic Resonance (EPR) Spectroscopy. Figure 3 shows the perpendicular-mode X-band EPR spectrum of F393H, recorded at 10 K using 2.01 mW microwave power. The g -values of features discussed are indicated on the figure. Minor signals at $g \approx 5.8$ and 4.3 are due to trace amounts of high-spin ferric heme and adventitious Fe^{III} ion, respectively. The three major features at $g = 2.43$, 2.25, and 1.92 are characteristic of a low-spin ferric heme and are virtually identical to those reported for the wild-type protein. These g -values are typical of native low-spin ferric P450s

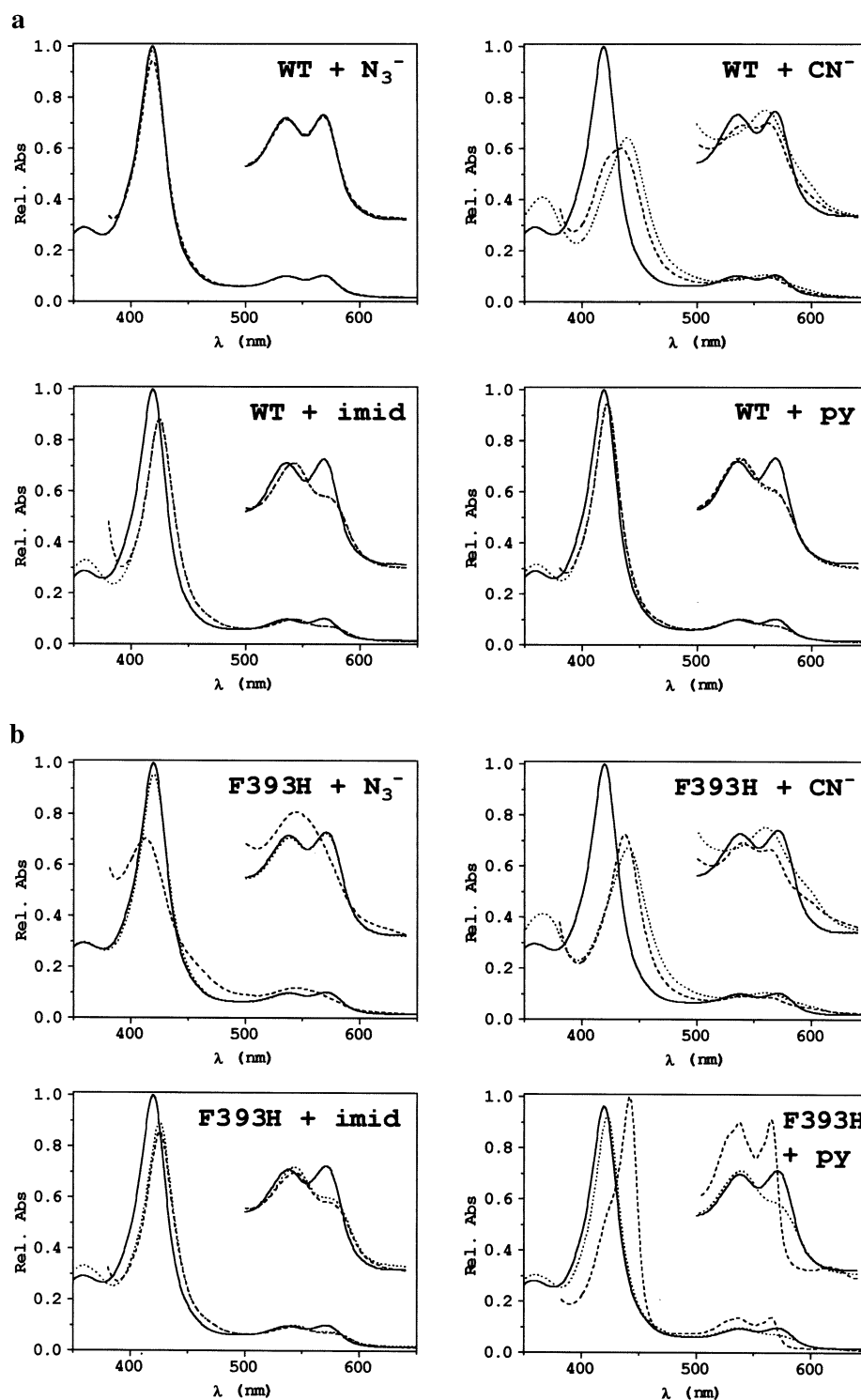


FIGURE 1: Visible spectra of azide (N_3^-), cyanide (CN^-), imidazole (imid), and pyridine (py) binding to wild-type P450 BM3 (Figure 1a) and to the F393H mutant (Figure 1b) in their oxidized (dotted line) and reduced (dashed line) ligand-bound forms. The spectra have been corrected to the same relative absorbance. The ligand-free, oxidized spectrum is also shown for each case (solid line) as a comparison.

and nitric oxide synthases (NOS) in which the heme is bound axially by cysteinate and water and also match those of adducts in which the water is displaced by a range of oxygen-donor ligands (27–31).

Determination of the F393H Crystal Structure. A data set to a resolution of 2.0 Å was used to refine the structure to a final *R*-factor of 17.9% (Table 4). The final model consists of two protein molecules, A and B, each containing residues Lys3–Leu188 and Asn201–Leu455, 1 heme, and a total of

1182 water molecules. For both molecules, the electron density for the first two N-terminal residues and the loop region containing residues Gln189–Glu200 was uninterpretable, so these have been omitted from the model. The rmsd fits [using the Dali server (32)] of all remaining Cα atoms for the wild-type and F393H-HD enzymes have been calculated using all possible combinations of molecules A and B in either model. The smallest difference (0.3) is found by comparing F393H-HD chain A with wild-type chain A,

Table 3: Spectral Characteristics of Ligand Binding to Wild-Type and F393H Mutant Cytochromes P450 BM3^a

	absorption maxima (nm)					
	P450 BM3 wild-type			P450 BM3 F393H		
	Soret	α	β	Soret	α	β
Fe ^{III}	419	569	536	419	571	538
Fe ^{III} -N ₃ ⁻	419	569	536	419	571	538
Fe ^{III} -CN ⁻	440	560*		440	560*	
Fe ^{III} -imidazole	425	573	543	426	576	543
Fe ^{III} -pyridine	422	568	538	423	572	538
Fe ^{II}	407	550*		413	554*	
Fe ^{II} -N ₃ ⁻	419	569	536	413	554*	
Fe ^{II} -CN ⁻	434	563	541	437	564	540
Fe ^{II} -imidazole	425	573	543	426	576	543
Fe ^{II} -pyridine	422	568	538	442	565	538

^a The table illustrates the positions of the major heme absorption bands [α , β , and γ (or Soret)] for ferric- and ferrous-forms of the enzymes in the absence and presence of exogenous ligands azide, cyanide, imidazole and pyridine. Asterisks denote fused absorbance bands whose components cannot be resolved into two separate contributions. Spectra were collected as described in the Experimental Procedures.

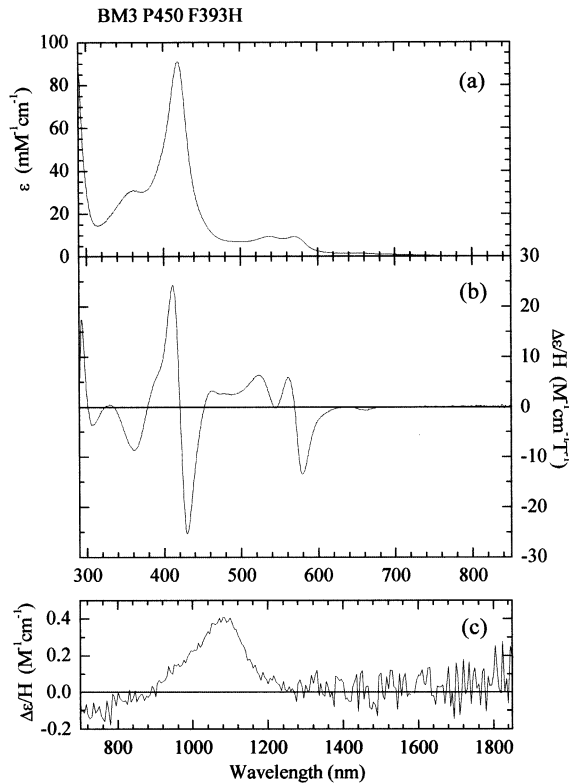


FIGURE 2: Spectral characteristics of P450 BM3 F393H heme domain, (a) electronic absorption spectrum, (b) UV-vis region MCD spectrum, (c) NIR-region MCD spectrum. MCD were recorded using a magnetic field of 6 T. MCD Sample concentration was 218 μ M.

and the largest (0.8) is found by comparison of F393H-HD chain A with wild-type chain B, indicating no significant structural differences. The regions surrounding residue 393 in the two structures is shown in Figure 4. Superposition of the phenyl ring of Phe393 from wild-type P450 BM3 onto His393 of F393H-HD molecule A is shown in Figure 5, and the comparison shows that the substitution causes little difference in the conformation of the residue side chain.

The only significant difference between the wild-type heme domain structure and the F393H-HD structure is the

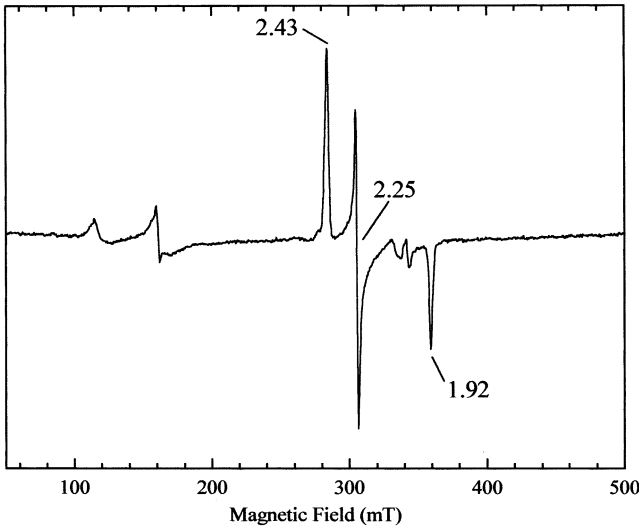


FIGURE 3: EPR spectrum of ferric P450 BM3 F393H heme domain. The spectrum was recorded at 10 K, using a 1 mT modulation and 2.01 mW microwave power. Sample concentration was 218 μ M. The g -values of 2.43, 2.25, and 1.92 are typical of low spin, ferric heme. Signals at $g \approx 5.8$ and 4.3 are due to small amounts of high spin ferric heme and adventitious iron.

Table 4: Crystallographic Data Statistics for the Crystal Structure of P450 BM3 Heme Domain Mutant F393H

refinement (\AA)	40.0–2.0
total no. of reflections	480 222
unique reflections	73 016
completeness (%)	96.9
$\langle I \rangle / \langle \sigma(I) \rangle$	19.4
$R_{\text{merge}} (\%)^a$	5.4
R_{merge} in outer shell (2.07–2.00) (%)	13.8
$R_{\text{cryst}} (\%)^b$	17.93
$R_{\text{free}} (\%)^b$	23.12
rmsd from restraint values	
bond length (\AA)	0.006
bond angle distance (\AA)	1.8
Ramachandran analysis	
most favored (%)	90.8
additionally allowed (%)	8.8

^a $R_{\text{merge}} = \sum |I - \langle I \rangle| / \sum I$ over all reflections. ^b $R_{\text{cryst}} = \sum |F_o - F_c| / F_o$; R_{free} calculated with 5.2% data withheld from refinement.

replacement of phenylalanine by histidine (Figure 5). The side chain of residue 393 is in a very similar position in both structures, sandwiched between the side chains of Pro392 and Gln403, with no major conformational changes of surrounding residues as a result of the mutation (Figure 6).

In the structure of the substrate-free wild-type heme domain, the distance of closest contact between Phe393 and Cys400 (the thiolate ligand to the heme iron) is 3.67 \AA , while in the structure of F393H-HD, the closest contact is between C δ 2 of the histidine side chain and C β of Cys400, a distance of 3.50 \AA (resulting from a slight tilt in the imidazole ring of H393, toward the heme ligand).

A possibility as to why the thermodynamic properties of the heme of the F393H mutant differ so much from wild-type is the ability for this histidine to be protonated and to form a hydrogen bond with Cys400 (analogous to the Trp...Cys hydrogen bond observed in NOS) (33). It can be seen from the structure of the mutant enzyme that there is a solvent water molecule (X526 in molecule A) positioned on the opposite side of His393 to the heme, which is hydrogen

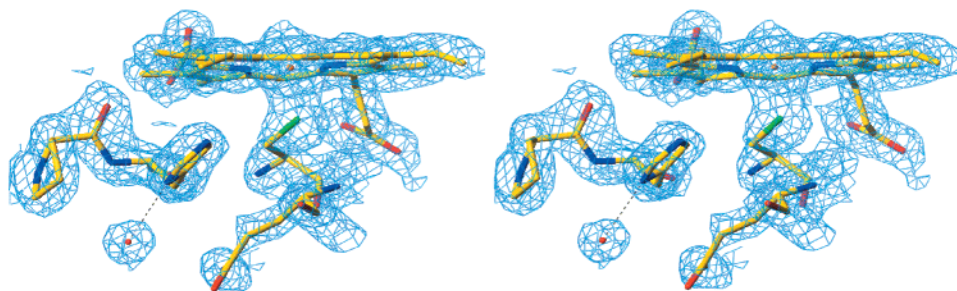


FIGURE 4: A stereoview of the heme binding region of the F393H mutant. Electron density is shown in cyan, while the heme macrocycle and peptide are shown in atom-type colors (red = oxygen, blue = nitrogen, and green = sulfur), the heme iron is depicted in orange. This figure clearly shows electron density for water molecule X and the likelihood of an intermolecular hydrogen bond to histidine 393. The electron density map was calculated using Fourier coefficients ($2F_o - F_c$), where F_o and F_c are the observed and calculated structure factors, respectively. The contour level is 1.5σ , where σ is the rms electron density. This diagram was generated using TURBO-FRODO (46).

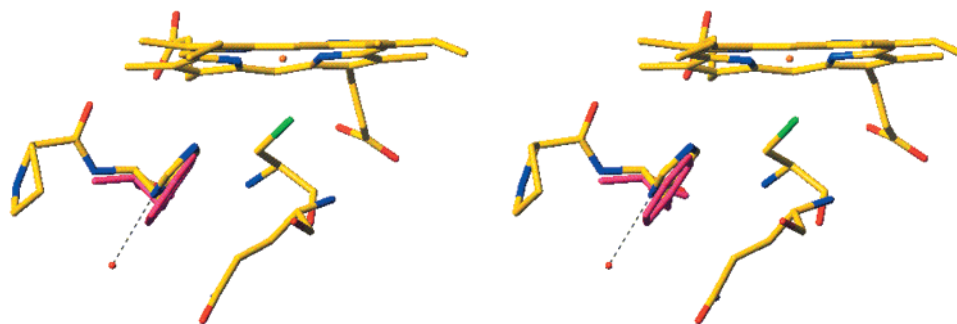


FIGURE 5: Superposition of phenylalanine 393 of wild-type P450 BM3 (magenta) onto histidine 393 of the F393H mutant. This clearly illustrates the minimal perturbation caused to the heme binding region by substitution of phenylalanine by histidine.

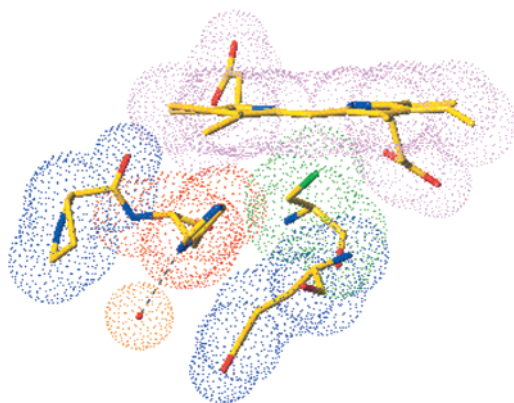


FIGURE 6: Constrained conformation of Phe393 in P450 BM3. The dotted regions describe the van der Waals surfaces of residues and the heme macrocycle surrounding histidine 393. The proximity of Pro392 and Gln403 prevents rotation of the imidazole ring of H393, precluding the possibility of the formation of an intramolecular H393...Cys400 hydrogen bond.

bonded to N δ 1 of the histidine side chain (N...O = 2.77 Å). The apparent protonation state of this histidine and the presence of an intermolecular hydrogen bond to water appears to preclude the formation of an intramolecular His393...Cys400 hydrogen bond.

DISCUSSION

Analysis of the F393H mutant of flavocytochrome P450 BM3 highlights the sensitivity of this enzyme to the nature of the residue at this position. Induced changes in the catalytic properties of the enzyme by substitutions at F393 suggest an important role for this residue, and have been discussed in detail in the previous paper (11). While the

effects on kinetic and thermodynamic properties have been experimentally substantiated, the physical process (i.e., the precise *cause*) by which these differences have occurred remained unresolved.

The product profile characterization of the F393H mutant confirmed the kinetics of NADPH oxidation described in the previous paper, with NADPH consumption being almost exclusively coupled to substrate turnover (~90% coupling) (11). Product analysis of the F393H mutant-catalyzed myristate-turnover was essentially identical to wild-type, with ω -1 hydroxylation predominating. No unusual oxidation products, suggestive of a change in the specificity of the mutant, were observed. From this we can conclude that F393 does not influence significantly the regio- and substrate-specificity of the enzyme. This is an important observation, confirming that F393H is able to act as a P450, yet is catalytically impaired relative to wild-type.

The EPR spectrum of the F393H mutant is identical to that of the wild-type enzyme. This infers that the iron in the ferric form is in a similar environment (no change in g values) in both enzymes and that they share a common ferric resting state. The form of the EPR spectrum is determined mainly by the relative splitting of the ferric d -orbitals, and if all five are moved in energy together by a process that does not substantially alter the iron geometry, then the spectrum would remain the same. It is surprising, therefore, that the elevation in the reduction potential of the heme does not induce a significant change in the EPR spectrum. This is our observation, which implies that the positive shift in the reduction potential of the F393H mutant relative to wild-type [reported previously (11)] is due to a difference in the energy of their ferrous-forms, relative to this common ferric ground state (Figure 7). Electrons are more easily introduced

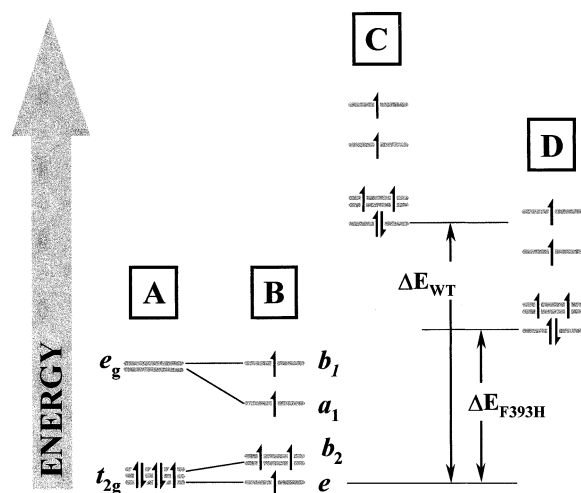


FIGURE 7: Diagrammatic representation of the proposed perturbation in the iron d -orbital energies between the ferric-resting state (A), the substrate-bound state (B), and the one-electron reduced forms of wild-type (C), and F393H mutant (D), caused by the substitution of phenylalanine 393 by histidine. The energy difference (ΔE) between the ferric- and ferrous- d -orbitals (related to the $\text{Fe}^{\text{III}}/\text{Fe}^{\text{II}}$ reduction potential by the Nernst equation, $\Delta G = -nF\Delta E$) is smaller for the F393H mutant (ΔE_{F393H}) than wild-type (ΔE_{WT}). This is consistent with the elevated reduction potential of the F393H mutant compared to the wild-type enzyme. The similarity of the ferric-EPR spectra for the F393H and wild-type enzymes suggest that the magnitude of the crystal field splitting parameter (Δ_o) is unchanged by the mutation.

to the iron frontier orbitals of the F393H mutant as a consequence of the difference in the energy (ΔE) between the ferric- and ferrous-forms being smaller than for wild-type. This is reflected in the $\text{Fe}^{\text{III}}/\text{Fe}^{\text{II}}$ couple for the F393H mutant being more positive than wild-type (reduction requires less energy). While this is an unusual observation, it is not unique. It has been demonstrated that loading the core of the bacterioferritin from *Azotobacter vinelandii* drops the reduction potential of its heme group by ~ 250 mV, without changes being observed in the EPR and MCD spectra of the loaded and unloaded forms (34). However, the most informative difference between wild-type and the F393H mutant is seen as a ~ 40 nm shift in the NIR charge transition in the MCD spectrum. This absorption has been assigned to a porphyrin (π) \rightarrow ferric (d) ligand to metal charge transition. The position of this band has been shown to vary greatly with axial ligation, for example a shift of ~ 350 nm is observed between a bis-his ligated (e.g., cytochrome c_3 , *Desulfovibrio vulgaris*) and met-his ligated (e.g., cytochrome b_{562} , *E. coli*) heme (26). Although we are concerned with a six coordinate cys-aqua ligated heme in P450s, a similar interpretation can be employed, whereby the shift in the NIR-CT band arises not as a result of a change in the nature of the ligation, but due to a change in the strength (as a consequence of a change in length) of the Fe–Cys bond. Although our observed shift is considerably smaller than that observed for a ligand change, it is large enough to be significant and consistent with a change in axial bond strength rather than bond type. Whether the change in the strength of the Fe–S bond is equivalent to the same magnitude of shift in the reduction potential observed between wild-type and the F393H mutant, is questionable.

The crystal structure of the F393H-HD mutant (solved to 2.0 Å) clearly shows the presence of the five-membered

imidazole ring of histidine, in place of the six membered phenyl ring of phenylalanine. This appears to be the only significant difference in the heme-binding region between the F393H mutant- and wild-type structures. Unfortunately, this does not help to explain how the presence of a histidine in place of a phenylalanine can so severely change the physical properties of the heme. No obvious conformational change is observed, and so the modification to the catalytic properties must be due to a more subtle, yet significant change in the protein superstructure or the way in which it interacts with the heme.

While inspection of the crystal structure does not immediately answer the question of how the reduction potential in the F393H mutant is being modulated, it does provide a structural context for discussion. The two dominant factors which influence reduction potentials in proteins are (a) the dielectric environment of the heme and (b) bonding interactions at, and to, the redox center (35). Both of these factors will be discussed in the context of the F393H mutant and in comparison with wild-type.

The study of the F393H mutant enzyme allows us to qualitatively evaluate how, or even if, changes in size, hydrophobicity, and electrostatics (due to the substitution of phenylalanine to histidine), affects the heme reduction potential. The Phe \rightarrow His substitution does not grossly increase the exposure of the heme to solvent, or dramatically change the hydrophobicity of the heme binding pocket. While the N δ 1 of the His393 is solvent exposed [formation of a His \cdots H $_2$ O H-bond (Figure 4)], the steric bulk of the histidine residue is sufficient to prevent the penetration of water which would alter the dielectric environment at the iron, and hence the redox properties, of the heme. The crystal structure was determined at pH 6.5, a pH at which His may be expected to be partially protonated, with the resulting imidazolium interacting with Cys400. Redox titrations of both wild-type and the F393H mutant have been performed over a pH range 6–8 (data not shown) and neither show a significant (<15 mV) deviation from the value of the reduction potential determined at pH 7.0. Since the redox potential of the F393H mutant is not pH dependent, one must conclude that His393 remains in the same protonation state through the pH range 6–8. How the His-water hydrogen bond affects the pK_a of this residue is unquantifiable, but if, for example, it is dramatically increased (i.e., toward the pK_a of free imidazole, $pK_a = 9$), it is plausible that the residue would have mainly imidazolium character within the range pH 6–8. The presence of a positive charge so close to the heme-ligand would introduce a significant electrostatic interaction between His393 and Cys400. This increase in Lewis acidity would destabilize the Fe–S bond, probably by drawing electron density away from the iron and toward His393 and have the concomitant effect of lengthening, hence weakening, the Fe–S bond.

On the basis of structural evidence, there is little conformational difference in the heme binding region between the F393H mutant and wild-type. In fact, this region of the F393H mutant is the most well-defined (conformationally) stretch of polypeptide compared to wild-type. It seems unlikely that the substitution of phenylalanine by histidine would cause a large enough change in the hydrophobicity or dielectric environment of the heme to account for the dramatic differences observed in the reduction potentials. The

comparison of cytochrome *c* with the octapeptide (methionine) complex (formed by the hydrolysis of cytochrome *c*) is the classic study of how heme solvation and the change in the dielectric environment of the heme affects redox properties (36). Here a heme reduction potential shift of 300 mV is observed between the semiexposed, partially solvated heme of cytochrome *c*, with the fully exposed and solvated heme of the octapeptide (hence, the difference in solvation being substantial and influential). It is also interesting to note that the reduction potential in a series of F82 mutants of cytochrome *c* (a highly conserved phenylalanine in cytochrome *c*, in a similar environment to F393 in P450 BM3) shift only slightly (by 43 mV) upon substitution of phenylalanine by glycine (37). Previously, the minor redox potential changes of these cytochrome *c* Phe82 mutants had been rationalized by assuming the removal of the steric bulk of phenylalanine was compensated for by a refolding of the peptide. While this resulted in a change in the dielectric environment of the heme (increased the number of polar amide backbone groups in the hydrophobic heme pocket, due to the refolding), no overall increase in the degree of heme solvation was observed compared to wild-type cytochrome *c* (38, 39). The fact the F393H mutant involves such a slight steric substitution suggests that the changes in hydrophobicity and heme-exposure, would be minimal compared to wild-type P450 BM3.

Distortions to the heme-plane would cause perturbations in the energy levels of the porphyrin macrocycle, leading to modifications of the thermodynamic properties of heme. Residue 393 is within van der Waals contact of the heme plane, so any increase or decrease in steric bulk at this position would have an impact on the degree of this interaction. How this change would manifest itself is unclear, but it is conceivable that the energy levels in the porphyrin could be perturbed. Direct comparison of heme planes is difficult, as the degree of distortion depends highly upon the constraints placed on the heme during refinement of the structure. Neither heme looks particularly distorted with no significant difference in the *b*-factor of the hemes between the two structures.

More plausible reasons for the modification of the redox properties observed are the factors affecting the bonding interactions of the redox center. The iron–cysteine bond is central to the reactivity of P450s. It has been suggested that the cysteinate ligand provides a “push” effect, whereby the strong electron donating nature of the thiolate pushes electron density toward the heme iron. This increases the heme electronegativity (40, 41), facilitating the stabilization of high iron oxidation states, and also helping the heterolytic cleavage of the O₂ bond. Therefore, it is likely that factors affecting the nature of the Fe–S bond are likely to have significant implications on the P450 catalytic cycle. In nitric oxide synthases (NOSs), there is a highly conserved tryptophan residue six residues downstream of the cysteine ligand, which forms an intramolecular hydrogen-bond with the heme ligand (33). The formation of such a bond in the F393H mutant would have the effect of removing electron density from the Fe–S bond, reducing the ability of the thiolate to stabilize high oxidation states. Alternatively, this thiolate can be considered as being more highly tuned to stabilizing low oxidation states [e.g., nNOS, $E_{1/2} = -239$ mV (42)]. Wild-type P450 BM3 does not have the potential to form a

Phe393...Cys400 hydrogen-bond, yet the F393H mutant does. The F393H mutant has an elevated reduction potential, which equates to as a more stable ferrous-form. The question is whether this increase in the reduction potential is due to His393 forming an intramolecular hydrogen bond to the cysteine or not. Our results suggest this might not be the case, for three different reasons. First, the His393...Cys400 distance is too long (3.5 Å) for an efficient hydrogen bond. Second, a region of electron density is observed between Nδ1 of His393 and a solvent water molecule, indicative of a protein–solvent hydrogen-bond. This does not immediately preclude the presence of an intramolecular hydrogen-bond, as the nature of the His393...H₂O bond is dependent on whether His393 is acting as the hydrogen-donor or hydrogen-acceptor, a feature undeterminable at the resolution of the crystal structure. Third, it would appear that the available sulfur lone pair is pointing in an orientation unsuitable for efficient hydrogen-bonding geometry with respect to His393. Such a hydrogen bond, if formed, would be severely strained.

Porphyrin complexes with sulfur donors as axial ligands have been studied as a method of modeling features specific to P450s, such as control of their spin-state, reduction potential, and activity (43). For these types of complexes, the length of the ferric Fe–S bond is in excess of 2.3 Å and can be assumed as the equilibrium length of an Fe–S bond (44, 45). In P450cam and BM3, this distance is significantly shortened to 2.17 and 2.05 Å, respectively. It is clear that the protein superstructure in these P450s forces this distance to a nonequilibrium value, holding the sulfur closer to the iron. This is likely to be a key to P450 reactivity. The artificially short and strained (unfavorable interaction with pyrrole nitrogens of the porphyrin) Fe–S bond exaggerates the electron donating nature of the sulfur, increasing the electronegativity of the heme iron. In wild-type P450 BM3, Phe393 is sandwiched between Gln403 and Pro392 which prevents rotation of the phenyl ring. In the F393H structure, His393 adopts the same sandwiched orientation but is slightly tilted toward Cys400. As a result of this, the imidazole ring moves closer to Cys400 [distance of closest contact F393-(H393)...Cys400 = 3.67 Å (3.50 Å)]. The increased steric interaction between His393 and Cys400 could lengthen the Fe–S bond, causing a decrease in the electronegativity of the iron. A comparison of the substrate-free heme-domain crystal structures of wild-type and the F393H mutant may lend some support to this suggestion. The Fe–S distances of wild-type and the F393H mutant are 2.05 and 2.13 Å, respectively, suggesting a slight increase in the bond length induced by the substitution of phenylalanine by histidine. However, at the resolution to which these structures have been solved (2.0 Å), the difference in the Fe–S bond lengths falls within the error associated with each bond (± 0.2 Å). Clearly, further investigation of this hypothesis is required before a formal conclusion can be drawn as to whether this increase in bond length is genuine. However, if it were, such a lengthening would account for the observed increased in redox potential.

CONCLUSION

The spectroscopic and structural comparison of wild-type and the F393H mutant of P450 BM3 has provided important information pertaining to the thermodynamic control exerted over the heme by phenylalanine 393. Our investigations have

shown that this control is achieved not by a gross conformational change in the heme binding region of the polypeptide. Rather, it arises as a consequence of a combination of a number of subtle, intimately linked factors. These include the close proximity of Phe393 to the heme porphyrin and to the cysteine ligand and their unavoidable interaction, its electrochemical neutrality, hydrophobicity, and ability to prevent exposure of the heme or the cysteine ligand to solvent.

ACKNOWLEDGMENT

Thanks is also due to Dr.'s S.N. Daff and L.J. Yellowlees for useful discussions and intellectual contributions.

REFERENCES

- Bower, S., Perkins, J. P., Yocum, R. R., Howitt, C. L., Rainham, P., and Pero, J. (1996) *J. Bacteriol.* 178, 4122–4130.
- Chung, B.-C., Matteson, K. J., Voutilainen, R., Mohandas, T. K., and Miller, W. L. (1986) *Proc. Natl. Acad. Sci. U.S.A.* 83, 8962–8966.
- Guengerich, F. P. (1995) Human Cytochrome P450 enzymes. In *Cytochrome P450: Structure, Mechanism and Biochemistry* (Ortiz de Montellano, P. R. O., Ed.) 2nd ed., pp 473–535, Plenum Press, New York.
- Chapman, S. K., Daff, S. N., and Munro, A. W. (1997) *Struct. Bonding* 88, 39–70.
- Shimizu, T., Hirano, K., Takahashi, M., Hatano, M., and Fujii-Kuriyama, Y. (1988) *Biochemistry* 27, 4138–4141.
- Sono, M., Roach, M. P., Coulter, E. D., and Dawson, J. H. (1996) *Chem. Rev.* 96, 2841–2887.
- Sono, M., Andersson, L. A., and Dawson, J. H. (1982) *J. Biol. Chem.* 257, 8308–8320.
- Miles, C. S., Ost, T. W. B., Noble, M. N., Munro, A. W., and Chapman, S. K. (2000) *Biochim. Biophys. Acta* 1543, 383–407.
- Gerber, N. C., and Sligar, S. G. (1994) *J. Biol. Chem.* 269, 4260–4266.
- Munro, A. W., Malarkey, K., McKnight, J., Thomson, A. J., Kelly, S. M., Price, N. C., Lindsay, J. G., Coggins, J. R., and Miles, J. S. (1994) *Biochem. J.* 303, 423–428.
- Ost, T. W. B., Miles, C. S., Munro, A. W., Murdoch, J., Reid, G. A., and Chapman, S. K. (2001) *Biochemistry* 40, 13421–13429.
- Song, W.-C., Funk, C. D., and Brash, A. R. (1993) *Proc. Natl. Acad. Sci. U.S.A.* 90, 8519–8523.
- Itoh, A., and Howe, G. A. (2001) *J. Biol. Chem.* 276, 3620–3627.
- Hara, S., Miyata, A., Yokoyama, C., Inoue, H., Brugger, R., Lottspiech, F., Ullrich, V., and Tanabe, T. (1994) *J. Biol. Chem.* 269, 19897–19903.
- Ohashi, K., Ruan, K.-H., Kulmacz, R. J., Wu, K. K., and Wang, L.-H. (1992) *J. Biol. Chem.* 267, 789–793.
- Miles, J. S., Munro, A. W., Rospendowski, B. N., Smith, W. E., McKnight, J., and Thompson, J. A. (1992) *Biochem. J.* 288, 503–509.
- Ravichandran, K. G., Boddupalli, S. S., Hasemann, C. A., Peterson, J. A., and Deisenhofer, J. (1993) *Science* 261, 731–736.
- Otwinowski, Z., and Minor, W. (1997) *Methods Enzymol.* 276, 307–326.
- Jones, T. A., Zou, J. Y., Cowan, S. W., and Kjeldgaard, M. (1991) *Acta Crystallogr., Sect. A* 47, 110–119.
- Sheldrick, G. M., and Schneider, T. R. (1997) *Methods Enzymol.* 277, 319–343.
- Ho, P. P., and Fulco, A. J. (1976) *Biochim. Biophys. Acta* 431, 249–256.
- Boddupalli, S. S., Estabrook, R. W., and Peterson, J. A. (1990) *J. Biol. Chem.* 265, 4233–4239.
- Williams, R. J. P. (1956) *Chem. Rev.* 5, 299–328.
- Cheesman, M. R., Greenwood, C., and Thomson, A. J. (1991) *Adv. Inorg. Chem.* 36, 201–255.
- Seward, H. S. (2000) Ph.D. Thesis, University of East Anglia.
- Gadsby, P. M. A., and Thomson, A. J. (1990) *J. Am. Chem. Soc.* 112, 5003–5011.
- Dawson, J. H., Andersson, L. A., and Sono, M. (1982) *J. Biol. Chem.* 257, 3606–3617.
- Berka, V., Palmer, G., Chen, P.-F., and Tsai, A. L. (1998) *Biochemistry* 37, 6136–6144.
- McKnight, J., Cheesman, M. R., Thomson, A. J., Miles, J. S., and Munro, A. W. (1993) *Eur. J. Biochem.* 213, 683–687.
- Salerno, J. C., Frey, C., McMillan, K., Williams, R. F., Masters, B. S. S., and Griffith, O. W. (1995) *J. Biol. Chem.* 270, 27423–27428.
- Tsai, A.-L., Berka, V., Chen, P.-F., and Plamer, G. (1996) *J. Biol. Chem.* 271, 32563–32571.
- Holm, L., and Sander, C. (1996) *Science*, 273, 595–602.
- Adak, S., Crooks, C., Wang, Q., Crane, B. R., Tainer, J. A., Getzoff, E. D., and Stuehr, D. J. (1999) *J. Biol. Chem.* 274, 26907–26911.
- Watt, G. D., Frankel, F. H. A., Al-Basseet, J., Al-Massad, F., Farrar, J., Greenwood, C., Thomson, A. J., and Moore, G. R. (1986) *Biochemistry* 85, 4330–4336.
- Moore, G. R., Pettigrew, G. W., and Rogers, N. K. (1986) *Proc. Natl. Acad. Sci. U.S.A.* 83, 4998–4999.
- Churg, A. K., and Warshel, A. (1986) *Biochemistry* 25, 1675–1681.
- Rafferty, S. P., Guillemette, J. G., Berghuis, A. M., Smith, M., Brayer, G. D., and Mauk, A. G. (1996) *Biochemistry* 35, 10784–10792.
- Louie, G. V., and Brayer, G. D. (1989) *J. Mol. Biol.* 209, 313–322.
- Rafferty, S. P., Pearce, L. L., Braker, P. D., Guillemette, J. G., Kay, C. M., Smith, M., and Mauk, A. G. (1990) *Biochemistry* 29, 9365–9369.
- Crane, B. R., Arvai, A. S., Gachhui, R., Wu, C., Ghosh, D. K., Getzoff, E. D., Stuehr, D. J., and Tainer, J. A. (1997) *Science* 278, 425–431.
- Ghosh, D. K., Wu, C., Pitters, E., Moloney, M., Werner, E. R., Mayer, B., and Stuehr, D. J. (1997) *Biochemistry* 36, 10609–10619.
- Presta, A., Weber-Main, A. M., Stankovich, M. T., and Stuehr, D. J. (1998) *J. Am. Chem. Soc.* 120, 9460–9465.
- Tani, F., Matsu-ura, M., Nakayama, S., Ichimura, M., Nakamura, N., and Naruta, Y. (2001) *J. Am. Chem. Soc.* 123, 1133–1142.
- Hahn, J. E., Hodgson, K. O., Andersson, L. A., and Dawson, J. H. (1982) *J. Biol. Chem.* 257, 10934–10941.
- Schappacher, M., Ricard, L., Fischer, J., Weiss, R., Bill, E., Montiel-Montoya, R., Winkler, H., and Trautwein, A. X. (1987) *Eur. J. Biochem.* 168, 419–429.
- Roussel, A., and Cambillau, C. (1991) *Silicon Graphics Geometry Partners Dictionary* 86, Silicon Graphics, Mountain View, CA.

BI010717E